JOURNAL OF CATALYSIS **165,** 184–196 (1997)
ARTICLE NO. CA971480

A Mo–K Edge XAFS Study of the Metal Sulfide-Support Interaction in (Co)Mo Supported Alumina and Titania Catalysts

R. G. Leliveld, A. J. van Dillen, J. W. Geus, and D. C. Koningsberger

Department of Inorganic Chemistry, Debye Institute, University of Utrecht, P.O. Box 80083, 3508 TB Utrecht, The Netherlands

Received April 23, 1996; revised July 24, 1996; accepted September 16, 1996

The metal-support interaction in oxidic and sulfided (Co)Mo/Al_2O_3 and (Co)Mo/TiO_2 catalysts has been studied with X-ray absorption spectroscopy. Analysis of the oxidic catalysts showed that on both Mo/Al_2O_3 and Mo/TiO_2 the molybdenum oxide particles possess a highly distorted octahedral structure with Mo–O distances ranging from 1.71 Å to 1.94 Å. The second shell Mo–Mo coordination number of less than 1.0 indicated that the size of the molybdenum oxide particles is very small. Upon addition of Co the particle size is increased to approximately four Mo atoms per particle. EXAFS data analysis showed the presence of second shell Al and Ti neighbours indicating a linkage of the molybdenum oxide particles to the support via Mo–O-*X* (*X* = Al or Ti) bonds. Upon sulfidation of the oxidic catalysts small MoS_2 particles are formed with second shell Mo–Mo coordination numbers ranging from 0.8 to 3.9. Å Mo–O contribution at 2.0 Å was found in the first coordination shell of Mo in the sulfided catalysts. Since the coordination number of this Mo–O contribution correlated with the MoS_2 particle size, deduced from the second shell Mo–Mo coordination number, this Mo–O contribution was assigned as an interfacial Mo–$O_{support}$ linkage. This Mo–$O_{support}$ linkage stabilises the small MoS_2 particles and prevents them from sintering. It is proposed that the activity of these catalysts can be controlled by optimising the molybdenum sulfide-support interaction, which consists of the observed Mo–$O_{support}$ bonds.

INTRODUCTION

Hydrotreating catalysts based on supported Co-, Ni-, and Mo-sulfides are among the most widely used catalysts. Although transition metal sulfides are already used in refineries since the late 1920s the interest in improving and understanding these catalysts is still high. A wealth of studies has been published on the structure and functioning of these kind of catalysts, as lately reviewed by several authors (1–14).

The structure and especially location of the active site is still a matter of debate. The generally accepted "CoMoS" model of Topsøe *et al.* (7) describes the active phase as consisting of small MoS_2 particles with Co promoter atoms decorating the edges of the MoS_2 slabs. Several EXAFS studies of Bouwens *et al.* (15–17) and extensive Mössbauer experiments by Crajé *et al.* (18–19) support this model and additionally indicate that the active sites are located on the cobalt atoms. The role of the MoS_2 particles is to act as a secondary support merely to stabilise the highly dispersed Co-sulfide located on the edges. Stabilisation of the MoS_2 slabs themselves is assumed to occur via Mo–O linkages to the support as proposed by several authors (17, 20–23).

The experimental evidence for the attachment of MoS_2 slabs to the support via Mo–O linkages is still not very convincing. Chiu *et al.* (24) attributed peaks in the Fourier transform of EXAFS data of a used $CoMo/Al_2O_3$ catalyst to two Mo–O contributions at 1.6 and 1.9 Å, respectively. Shimada *et al.* (25) reported a similar Mo–O contribution around 2.0 Å in the Fourier transform of a sulfided Mo/Al_2O_3 catalyst. However, both authors ascribed these Mo–O contributions to nonreducible oxygens and did not link them to the proposed Mo–O linkages between support and MoS_2 particles. Derouane *et al.* (26) indicated with the help of EPR the presence of similar oxo-molybdenum species resistant towards sulfiding and stabilising the MoS_2 particles. The most concrete evidence for the existence of Mo–O–Al linkages in MoS_2/Al_2O_3 was obtained by Diemann *et al.* (27) with the help of inelastic tunnelling spectroscopy.

A good understanding of the interaction between support and active phase and the effect on dispersion and activity of these catalysts is crucial. Knowledge of the nature of this interaction and the parameters that influence it will help in a further understanding and optimisation of these catalysts. The aim of this study, therefore, is to use EXAFS spectroscopy to elucidate the interaction between the MoS_2 particles and the surface of an oxidic support. In structural studies of the metal–support interface in supported noble metal catalysts EXAFS has proven to be a very suitable tool (28). This study will demonstrate that also in the study of structurally more complex systems like metal sulfides supported on oxidic supports EXAFS can be very helpful in the study of the metal sulfide-support interface, provided that catalysts with highly dispersed MoS_2 particles are used. As the final dispersion of the MoS_2 phase and the interfacial bonding with the support is likely to be influenced by

0021-9517/97 $25.00

the nature of the precursor catalyst, the structure of the oxidic catalysts was also analysed. It will be shown that the interaction between the Mo phase and the surface of the support is already present and detectable in the oxidic catalysts.

To study the effect of the support and to obtain variations in the metal–sulfide support interaction both Mo/Al_2O_3 and Mo/TiO_2 catalysts have been investigated. Recent studies indicate that Mo/TiO_2 catalysts have a higher intrinsic activity than Mo/Al_2O_3 catalysts, which is ascribed to a specific effect of the support on the active phase (29–30). Additionally, the pretreatment of the catalysts prior to sulfidation was varied to create extra variations in the active phase–support interaction. As most catalysts contain Co as promoter, the influence of Co on the structure of MoS_2 and its attachment to the support was studied too. Temperature programmed sulfiding studies by Moulijn *et al.* (31) have shown that Co eases the sulfiding of Mo, which may be ascribed to a diminished interaction between the MoS_2 slabs and the support.

METHODS

Preparation of the Catalysts

A 15 wt% MoO_3/γ-Al_2O_3 and a 4.4 wt% MoO_3/TiO_2 catalyst were prepared by incipient wetness impregnation of preshaped bodies of γ-Al_2O_3 (Ketjen CK-300, surface area 200 m^2/g, pore volume 0.63 ml/g) and TiO_2 (Degussa 7702, surface area 44 m^2/g, pore volume 0.14 ml/g, 80% anatase), respectively, with a solution of $(NH_4)_6Mo_7O_{24}\cdot 6H_2O$ (Merck, p.a.) containing 25% ammonia. The surface loading in both catalysts was 0.70 mg Mo/m^2 (monolayer coverage). The catalysts were subsequently dried in an air flow during 4 h at 25°C and for 16 h in static air at 110°C. To study the effect of calcination samples of each catalyst were calcined in air at 450°C for 16 h. The noncalcined samples are denoted by Mo/TiO_2(nc) and Mo/Al_2O_3(nc), respectively; the calcined samples are indicated by Mo/TiO_2(cal) and Mo/Al_2O_3(cal).

A $CoMo/Al_2O_3$ (3.8 wt% Co_3O_4, 14 wt% MoO_3) and $CoMo/TiO_2$ (1.1 wt% Co_3O_4, 4.3 wt% MoO_3) were prepared by impregnation of noncalcined Mo/Al_2O_3 and Mo/TiO_2 with an aqueous solution of $Co(NO_3)_3\cdot 6H_2O$ (Merck, p.a.). These catalysts are indicated by $CoMo/Al_2O_3$(seq) and $CoMo/TiO_2$(seq). Co-impregnated CoMo catalysts were prepared by impregnation of γ-Al_2O_3 and TiO_2 with an aqueous solution containing the required amounts of $(NH_4)_6Mo_7O_{24}\cdot 6H_2O$ and $Co(NO_3)_3\cdot 6H_2O$. All catalysts were subsequently dried in an air flow for 4 h at 25°C, dried in static air at 110°C for 16 h and calcined in air at 450°C during 16 h. The co-impregnated catalysts are denoted by $CoMo/Al_2O_3$(co) and $CoMo/TiO_2$(co), respectively.

EXAFS Data Collection

The EXAFS measurements were performed at EXAFS station 9.2 of the Wiggler beam line of the SRS in Daresbury (UK). The Si[220] double crystal monochromator was detuned to 50% intensity to minimise the presence of higher harmonics. Due to a reconstruction of the station, the co-promoted catalysts were measured with a spare channel cut Si[220] monochromator which could not be detuned. The decrease in photon flux at higher energies of the synchrotron radiation makes the contribution of the higher harmonics rather small, so it is not likely that the data are influenced by the use of the channel cut monochromator. The measurements were all carried out in transmission mode using optimised ion chambers as detectors. To minimise high- and low-frequency noise the counting time per data point was varied from 1 s at $k = 3$ Å^{-1} to 3 s at $k = 20$ Å^{-1} and at least three scans were recorded and averaged. All spectra were recorded with the sample at liquid nitrogen temperature. The energy calibration was performed by means of a Mo-foil placed in series with the sample using a third ionisation chamber. The absolute value of the Mo-edge is 19,999 eV.

The catalyst samples were pressed into self-supporting wafers and mounted in an in situ EXAFS cell (32). The thickness of the wafer was chosen to give an absorbance (μx) of 2.5 for optimal signal to noise ratio. To prevent thickness effects for the high loaded Mo/Al_2O_3 samples μx was set to yield a step of 1.0 in absorbance in the edge region. The wafers were dried in situ at 120°C for 1 h in a He flow (flow rate 50 ml/min^{-1}) after which an EXAFS spectrum of the Mo–K edge was recorded. The sulfidation of the catalysts was carried out in a 10% H_2S/H_2 flow (flow rate 50 ml/min^{-1}) while the temperature was linearly increased from 25°C to 400°C (5°C/min). The samples were kept at 400°C for 30 min and cooled down to room temperature (10°C/min). The cell was flushed for 15 min with He to remove H_2S after which the EXAFS spectrum was recorded. The Co-promoted catalysts were sulfided at 450°C as also, for reason of comparison, a Mo/Al_2O_3 and Mo/TiO_2 catalyst.

EXAFS Data Analysis

Standard procedures were used to extract the EXAFS data from the measured absorption spectrum. Normalisation was done by dividing the data by the height of the absorption edge and the background was subtracted using cubic spline routines (33). Phase shifts and backscattering amplitudes obtained from reference compounds were used to calculate the EXAFS contributions: $Na_2MoO_4\cdot 2H_2O$ for the Mo–O, and MoS_2 for the Mo–S and Mo–Mo contribution. Details of the references are described elsewhere (15). Phase shifts and backscattering amplitudes for the Mo–Al and Mo–Ti contributions were theoretically calculated with

the FEFF-3.1 program. Multiple shell fitting of the EXAFS data was done in *R*-space.The difference file technique was applied, together with phase-corrected Fourier transforms to resolve the different contributions (34). Coordination numbers were corrected for the difference in absorber-backscatterer distance between the reference compound and the unknown assuming an electron mean free path of 5 Å (35).

The reliability of the calculated fit is usually expressed as the goodness of fit ε_ν^2 which includes the statistical noise on the data (36). However, it proved that the random noise in some spectra is that low that $\varepsilon_\nu^2 \gg 1$. In that case the noise is dominated by systematic errors from the measurement and data analysis. To correct the standard deviations of the structural parameters for the systematic errors ε_ν^2 should be corrected as described by Stern *et al.* (37). The analysis program used, however, is not yet capable of performing this kind of statistical analysis. Alternatively we have chosen to express the quality of fit as the difference between the absolute or imaginary part of the Fourier transform of the experimental data with that of the model Fourier transform. These differences are described by the FT^n variance

$$FT^n = 100\frac{\int \left(FT^n_{model}(R) - FT^n_{expt}(R)\right)^2}{\int \left(FT^n_{expt}(R)\right)^2} \qquad [1]$$

in which n represents the weight of the Fourier transform. The errors in the resulting fit parameters are estimated to be 20% in coordination number N, 1% in distance R, 10% in Debye–Waller factor $\Delta\sigma^2$, and 10% in ΔE_0.

RESULTS

Data-Analysis of the Oxidic Catalysts

The near-edge spectra of the reference compound $Na_2MoO_4{\cdot}2H_2O$ and of Mo/Al_2O_3(cal), Mo/Al_2O_3(nc), Mo/TiO_2(cal), and Mo/TiO_2(nc) are shown in Fig. 1. The preedge peak present in the spectrum of all samples can be attributed to a 1s–4d bound state transition. The transition probability of this formally forbidden excitation is dependent on the local symmetry of the molybdenum atom. The effective mixing of metal d-states with ligand p-orbitals in case of tetrahedral symmetry gives rise to the intense preedge feature observed with $Na_2MoO_4{\cdot}2H_2O$ (38). In case of a nonperfect octahedral surrounding of the central atom the 1s–4d transition is only slightly allowed (39). The lower intensity of the preedge peaks in the spectra of the catalysts therefore points to a distorted octahedral coordination around the molybdenum atom as observed with, e.g., MoO_3. As can be seen in Fig. 1 there are only small differences between the intensities of the preedge peaks of the various catalysts. A small decrease is observed between Mo/Al_2O_3(nc) and Mo/Al_2O_3(cal) indicating a more centro-symmetric surrounding around the molydenum atom upon calcination (40). Comparison of Mo/TiO_2(nc) and Mo/TiO_2(cal) shows the opposite trend; i.e., the centro-symmetry around the molydenum atom decreases upon calcination. The Mo/TiO_2 samples have a slightly lower preedge feature than Mo/Al_2O_3 samples. This can be ascribed to a higher percentage of tetrahedral coordinated molybdenum oxide species on the alumina support as compared to the titania supported catalyst or alternatively to a less distorted octahedral structure on titania. The Mo/Al_2O_3(cal) and Mo/TiO_2(cal) catalysts promoted with Co show the same near-edge spectra as the unpromoted catalysts.

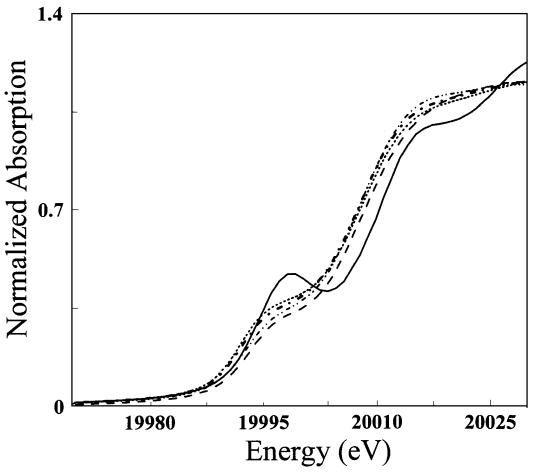

FIG. 1. XANES spectra of $Na_2MoO_4{\cdot}2H_2O$ (———), Mo/Al_2O_3(cal) (-·-·-), Mo/Al_2O_3(nc) (- - -), Mo/TiO_2(cal) (···), and Mo/TiO_2(nc) (– –).

Tables 1–3 contain the Fourier transform and analysis ranges of the EXAFS data of the catalysts and crystalline MoO_3, along with the fit parameters of the (Co) Mo catalysts. In Fig. 2a the absolute part of the Fourier transforms of the reference compound $Na_2MoO_4{\cdot}2H_2O$ and crystalline MoO_3 are displayed. The Fourier transform of $Na_2MoO_4{\cdot}2H_2O$ contains one large peak corresponding to four oxygen neighbours at 1.77 Å (41). The amplitude of the Mo–O contributions in MoO_3 is strongly reduced, compared to that of $Na_2MoO_4{\cdot}2H_2O$. This is the result of strong interference between the different Mo–O shells present in MoO_3. According to XRD analysis the molybdenum atom in MoO_3 is octahedrally surrounded by six oxygen atoms at 1.67, 1.73, 1.95 (2x), 2.25, and 2.33 Å (42). The EXAFS spectrum of MoO_3 can be fitted with three Mo–O shells at 1.70 (2x), 1.95 (2x), and 2.25 Å (2x) as displayed in Fig. 2b. Representing these contributions in *k*-space (Fig. 2c) it can be seen that the Mo–O shells at 1.70 and 1.95 Å differ almost $\pi/2$ in phase, leading to the observed lower amplitude of the Mo–O contributions in the Fourier transform. The EXAFS analysis of crystalline MoO_3 clearly illustrates the destructive interference between different Mo–O shells which can occur in complex molybdenum oxide structures. Fitting of both magnitude and imaginary parts of the Fourier

TABLE 1

Fourier Transform and Analysis Ranges Oxidic Catalysts

Sample	FT range Δk (Å^{-1})	Anal. range ΔR (Å)	Fit weight k^n	N_{indp}[a]	ν[b]	Var. abs. part FT[c]	Var. im. part FT[c]
Mo/Al_2O_3(nc)	4.0–13.7	0.5–5.0	2	21.4	1.4	0.56	2.55
Mo/Al_2O_3(cal)	4.0–12.0	0.5–4.0	2	18.8	2.8	1.04	2.34
$CoMo/Al_2O_3$(seq)	3.7–12.5	0.5–4.0	2	20.6	0.6	0.25	0.59
$CoMo/Al_2O_3$(co)	3.7–12.5	0.5–4.0	2	20.6	0.6	0.19	0.39
Mo/TiO_2(nc)	4.5–13.7	0.5–5.0	2	22.1	6.1	1.78	3.74
Mo/TiO_2(cal)	4.2–14.0	0.5–5.0	2	29.1	9.1	4.10	8.12
$CoMo/TiO_2$(seq)	3.7–12.5	0.5–4.0	2	20.6	0.6	0.49	0.95
$CoMo/TiO_2$(co)	3.7–12.5	0.5–4.0	2	20.6	0.6	1.66	2.28
MoO_3	3.9–13.7	0–2.2	2	15.0	3.0	2.04	10.0

[a] N_{indp} is number of independent parameters: $N_{indp} = 2\Delta k \Delta r/\pi + 1$.
[b] ν is degrees of freedom: $\nu = N_{indp} - N_{fit}$.
[c] See Eq. (1).

transform in *R*-space facilitates determination of the different Mo–O contributions compared to a fit in *k*-space. In general, fitting in *R*-space avoids truncation errors that are made when Fourier filtering is used (43). Moreover, an advantage of *R*-space fitting is the separate optimization of the magnitude and imaginary part of the Fourier transform. Modelling of the imaginary part improves the sensitivity for the distance *R*, which makes the optimization more sensitive for deconvolution of contributions that are not well separated (44).

In Fig. 3 the raw EXAFS data and k^1 Fourier transform of bulk MoO_3 and the Mo/Al_2O_3(cal) and Mo/TiO_2(cal) catalysts are shown. The amplitudes of the Mo–O contributions present at low values of R ($0 < R < 2.2$ Å) in the Fourier transform of the catalysts are comparable to those of MoO_3 and much lower than for $Na_2MoO_4{\cdot}2H_2O$. This

TABLE 2

Fit Parameters Oxidic Alumina Supported Catalysts and MoO_3

Scatterer	N	$\Delta\sigma^2$ (10^{-4}Å^2)	R (Å)	ΔE_0 (eV)
MoO_3				
O	1.9	16.1	1.70	1.6
O	2.2	11.3	1.95	4.3
O	2.4	41.9	2.25	8.1
Mo/Al_2O_3(cal)				
O	3.4	34.1	1.76	−7.9
O	2.6	43.2	1.92	9.0
Al	0.4	52.9	2.76	−15.0
Mo	0.4	59.8	3.28	8.7
$CoMo/Al_2O_3$(seq)				
O	1.8	24.9	1.71	−1.9
O	1.7	38.0	1.77	−0.9
O	1.6	29.2	1.94	5.5
Al	1.0	68.2	2.74	−9.1
Mo	1.4	58.0	3.31	9.8
$CoMo/Al_2O_3$(co)				
O	1.2	9.6	1.71	−3.4
O	2.4	49.5	1.77	−2.6
O	1.8	39.2	1.94	6.6
Al	1.1	91.4	2.74	−9.0
Mo	1.5	59.8	3.31	9.9
Mo/Al_2O_3(nc)				
O	2.2	40.4	1.71	−8.6
O	2.0	25.6	1.77	−0.6
O	1.6	34.7	1.94	0.8
Al	0.5	58.6	2.72	−10.2
Mo	0.7	67.6	3.29	3.5

TABLE 3

Fit Parameters Oxidic Titania Supported Catalysts

Scatterer	N	$\Delta\sigma^2$ (10^{-4}Å^2)	R (Å)	ΔE_0 (eV)
$Mo/TiO_{2(nc)}$				
O	3.0	16.7	1.74	−10.4
O	2.7	20.9	1.88	9.3
Mo	0.9	53.7	3.00	−6.8
Mo/TiO_2(cal)				
O	2.4	4.9	1.73	−10.0
O	2.4	18.1	1.89	5.2
Ti	0.3	10.4	2.83	−4.7
Mo	0.7	45.3	3.37	3.4
Mo	0.60	−21.2	3.72	10.0
$CoMo/TiO_2$(seq)				
O	0.7	10.3	1.71	1.7
O	2.2	47.9	1.74	2.6
O	0.9	29.0	1.94	6.2
Ti	0.2	−59.6	2.88	−7.6
Mo	1.8	82.3	3.40	−1.7
$CoMo/TiO_2$(co)				
O	2.3	27.3	1.72	2.6
O	0.7	71.2	1.78	1.6
O	1.4	97.3	1.92	7.1
Ti	0.1	−110.1	2.88	−8.0
Mo	2.5	76.7	3.41	−4.1

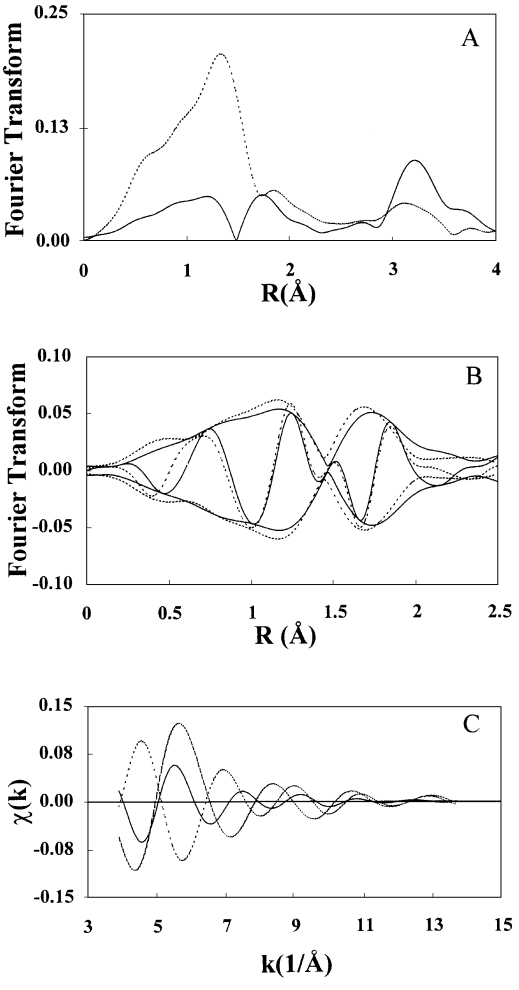

FIG. 2. (a) Fourier transform of $Na_2MoO_4{\cdot}2H_2O$ (---) and MoO_3 (———) [k^1, $\Delta k = 4.0-14.0$]. (b) Fourier transform of MoO_3 (———) and fit (---) [k^1, $\Delta k = 3.9-13.7$]. (cal) EXAFS spectrum of calculated Mo–O contributions at 1.70 Å (– – –), 1.95 Å (- - - -), and 2.25 Å (———).

indicates a complex octahedral structure of the molybdenum oxide particles with interfering Mo–O distances around 1.7 and 1.9 Å. Tables 2 and 3 present the coordination parameters used to obtain the best fit in *R*-space. The spectra can be fitted with Mo–O shells ranging from 1.69 to 1.95 Å. The fits are not perfect, due to the described interference between the different Mo–O shells and the variety in Mo–O bond lengths of the distorted octahedral molydenumoxide species. Moreover, it is quite possible as indicated by the near-edge spectra, that part of the Mo atoms are located in an tetrahedral structure. Nevertheless it is very clear that none of the catalysts can be fitted with a same set of parameters, illustrating that the structure of the molybdenum oxide particles is different on all catalysts. These differences are thus influenced by pretreatment, nature of support, and presence of a promoter.

Compared to MoO_3 the second shell in the Fourier transform (2.7–3.6 Å) of the catalyst samples is much lower in amplitude. The amplitude of this shell, which mainly consists of Mo–Mo contributions, is a measure for the size of the molybdenum oxide particles. The observed low amplitude indicates that in all catalysts the molybdenum oxide is very well dispersed on the support. Besides the Mo–Mo contribution a second contribution is observed in most spectra between 2.3 and 2.9 Å. This contribution could not be fit with a Mo–Mo shell, but incorporation of a Mo–Al or Mo–Ti shell led to satisfying results. Figures 4 and 5 presents the Fourier transforms for Mo/Al_2O_3(cal) and Mo/TiO_2(cal) and the best fits, together with the Fourier transforms of the difference files (raw data minus Mo–O and Mo–Mo contributions) and the calculated Mo–Al or Mo–Ti contribution, respectively. The distance between Mo and the Al atom of the support ranges from 2.72 to 2.76 Å. In Mo/TiO_2(cal) the Mo–Ti distance ranges between 2.83 and 2.88 Å.

Data-Analysis of the Sulfided Catalysts

In Table 4 the Fourier transform and analysis ranges of the EXAFS data are presented for the sulfided (Co)Mo catalysts. Figure 6a represents the raw data of

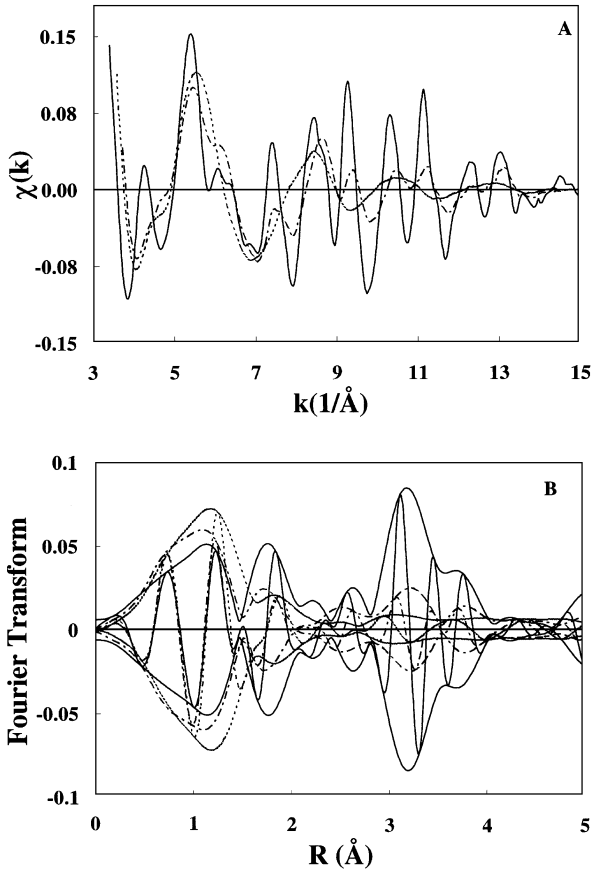

FIG. 3. EXAFS spectrum and Fourier transform of Mo/Al_2O_3(cal) (- - - - - -), Mo/TiO_2(cal) (- - - - -), and MoO_3 (thick solid line): (a) EXAFS spectrum; (b) Fourier transform [k^1, $\Delta k = 4.0-12.5$].

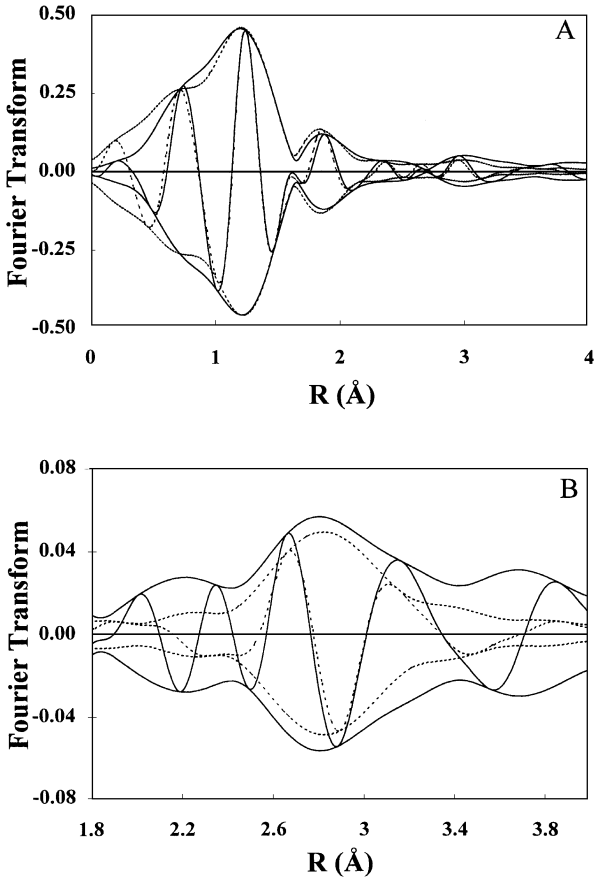

FIG. 4. (a) Fourier transform of Mo/Al_2O_3(cal) (———) and fit (- - -) [k^2, $\Delta k = 4.0-12.0$]; (b) Mo–Al contribution in Mo/Al_2O_3(cal), Fourier transform [k^2, $\Delta k = 4.0-12.0$]. EXAFS minus calculated Mo–O and Mo–Mo contributions (———) and fit with calculated Mo–Al contribution (- - -).

Mo/Al_2O_3(cal) and Mo/TiO_2(cal), sulfided at 400°C. The low noise level at high k-values illustrates the high data quality. In the Fourier transforms of these samples (Fig. 6b), displayed together with crystalline MoS_2, mainly two shells are present due to Mo–S and Mo–Mo contributions. In crystallinic MoS_2 with a hexagonal structure each Mo atom is surrounded by six sulfur atoms at 2.41 Å and by six molybdenum neighbours at a distance of 3.16 Å (45). The low amplitude of the Mo–Mo shell in the Fourier transform of both catalysts compared to that of crystalline MoS_2 shows that the supported MoS_2 particles are very small. The amplitude of the Mo–S shell is also strongly reduced with respect to that of MoS_2.

The coordination parameters obtained from the fitting procedure of the sulfided alumina and titania samples are given in Tables 5 and 6. To obtain a good fit of the second shell in Mo/TiO_2(cal) a Mo–Ti contribution had to be included. In Mo/Al_2O_3(cal) the incorporation of a Mo–Al contribution gave no improvement of the fit compared to the fit with only a Mo–Mo contribution. Figure 7a shows the Fourier transform of Mo/TiO_2(cal) and the best fit with three shells. It is a clear that this fit, including Mo–S, Mo–Mo, and Mo–Ti contributions strongly deviates from the experimental data at low r-values. When the Mo–S, Mo–Mo, and Mo–Ti contributions are subtracted from the raw experimental data the remaining contribution, or the so-called difference file, is obtained. As displayed in Fig. 8a the difference file could be perfectly fitted with a Mo–O contribution at 2.00 Å. Only between 0.7 and 1.5 Å and extra contribution remains, which is due to the atomic background. The positive maximum of the imaginary part of the Mo–O phase corrected Fourier transform justifies the fit with a Mo–O contribution. Alternatively this contribution could be fitted with a Mo–S contribution, but as Mo–S and Mo–O differ $\pi/2$ in phase the maximum of the imaginary part of the Fourier transform would then be negative in a Mo–O phase corrected Fourier transform. Also the distance of this contribution is unusually low for a Mo–S contribution. The statistical significance of the extra Mo–O shell should normally be determined by applying a F-test

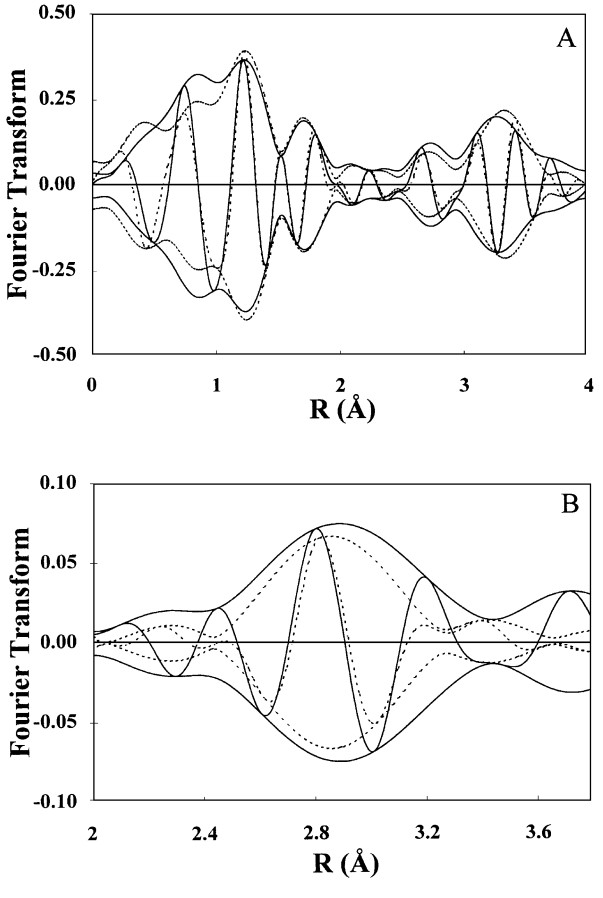

FIG. 5. (a) Fourier transform of Mo/TiO_2(cal) (———) and fit (- - -) [k^2, $\Delta k = 4.0-14.0$]; (b) Mo–Ti contribution in Mo/TiO_2(cal), Fourier transform [k^2, $\Delta k = 4.0-14.0$]. EXAFS minus calculated Mo–O and Mo–Mo contributions (———) and fit with calculated Mo–Ti contribution (- - -).

TABLE 4

Fourier Transform and Analysis Ranges Sulfided Catalysts

Sample	FT-range Δk (Å^{-1})	Anal. range ΔR (Å)	Fit weight k^n	N_{indp}[a]	ν[b]	Var. abs. part FT[c]	Var. im. part FT[c]
Mo/Al_2O_3(nc)	3.9–13.5	1.0–3.5	2	17.3	5.3	0.19	0.36
Mo/Al_2O_3(cal)	3.9–13.5	1.0–3.8	2	19.1	7.1	0.22	0.45
Mo/Al_2O_3(cal) 450°C	3.9–11.0	1.0–3.5	2	13.3	1.3	0.08	0.26
$CoMo/Al_2O_3$(seq)	3.9–11.0	1.0–3.5	2	13.3	1.3	0.06	0.19
$CoMo/Al_2O_3$(co)	3.9–11.0	1.0–3.5	2	13.3	1.3	0.09	0.25
Mo/TiO_2(nc)	3.9–13.5	1.0–3.8	2	19.1	7.1	0.34	0.63
Mo/TiO_2(cal)	3.9–13.0	1.0–3.8	2	18.2	2.2	0.31	0.48
Mo/TiO_2(cal) 450°C	3.9–11.0	1.0–3.5	2	19.0	3.0	0.08	0.16
$CoMo/TiO_2$(seq)	3.9–11.0	1.0–3.5	2	13.3	1.3	0.06	0.19
$CoMo/TiO_2$(co)	3.9–11.0	1.0–3.5	2	13.3	1.3	0.13	0.26

[a] N_{indp} is number of independent parameters: $N_{indp} = 2\Delta k \Delta r/\pi + 1$.
[b] ν is degrees of freedom: $\nu = N_{indp} - N_{fit}$.
[c] See Eq. (1).

on the ε_ν^2 values (36). However, the large ε_ν^2 values obtained for these data as explained above prohibit this approach. In Fig. 8b both the raw EXAFS data minus the Mo–S, Mo–Mo, and Mo–Ti contributions and the calculated Mo–O contribution are presented in *k*-space. The peak to peak noise of these data is lower than 0.001. As can be seen the Mo–O contribution is well above this noise level which signifies the reliability of this extra shell. The remaining deviation in *k*-space between the difference file and the calculated Mo–O contribution can be attributed to the earlier mentioned atomic background. In the data of all other catalysts a similar Mo–O contribution was found between 1.95 and 2.0 Å.

The best fit of the data of Mo/TiO_2(cal) with four shells including the Mo–O shell is presented in Fig. 7b. Compared to the fit with only three shells (Fig. 7a) the quality of the fit

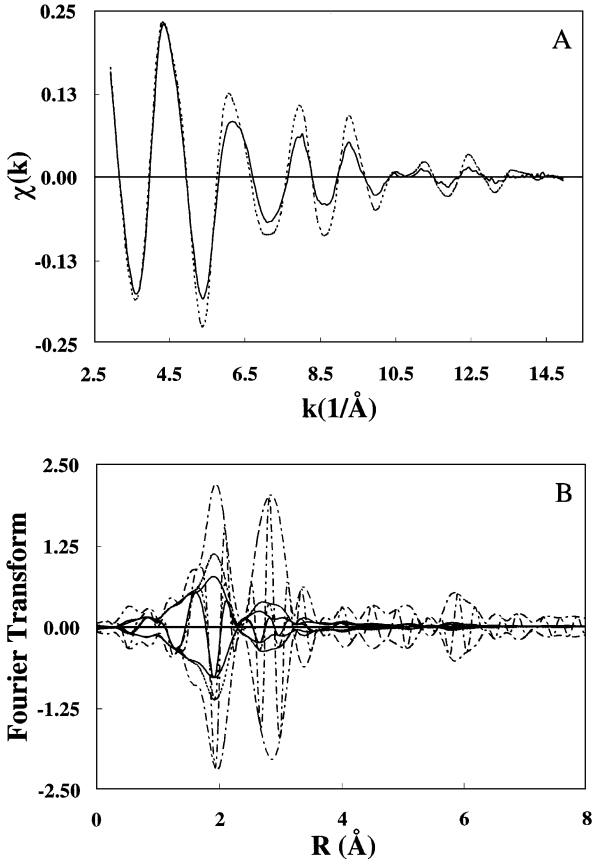

FIG. 6. (a) EXAFS spectrum of sulfided Mo/Al_2O_3(cal) (- - -) and Mo/TiO_2(cal) (———); (b) Fourier transform of sulfided Mo/Al_2O_3(cal) (- - -) and Mo/TiO_2(cal) (———) and MoS_2 (-·····-) [k^2, $\Delta k = 3.2–13.5$].

TABLE 5

Fit Parameters Sulfided Alumina Supported Catalysts

Scatterer	*N*	$\Delta\sigma^2$ (10^{-4}Å^2)	*R* (Å)	ΔE_0 (eV)
Mo/Al_2O_3(nc)				
O	0.6	27.4	2.00	0.0
S	4.7	22.1	2.40	4.7
Mo	2.9	36.4	3.15	3.6
Mo/Al_2O_3(cal)				
O	0.8	41.7	1.98	6.6
S	4.0	21.1	2.40	3.7
Mo	2.4	36.9	3.15	3.0
Mo/Al_2O_3(cal) 450°C				
O	0.6	28.7	1.99	−0.4
S	5.0	13.5	2.40	3.9
Mo	3.7	29.3	3.15	3.2
$CoMo/Al_2O_3$(seq)				
O	0.5	34.0	1.95	2.0
S	5.6	22.3	2.40	3.3
Mo	3.8	38.2	3.15	2.7
$CoMo/Al_2O_3$(co)				
O	0.5	42.8	1.95	7.4
S	5.5	20.8	2.41	2.3
Mo	3.9	40.9	3.15	3.3

TABLE 6

Fit Parameters Sulfided Titania Supported Catalysts

Scatterer	N	$\Delta\sigma^2$ (10^{-4}Å^2)	R (Å)	ΔE_0 (eV)
Mo/TiO_2(nc)				
O	1.2	66.3	2.00	1.6
S	3.9	20.5	2.40	2.4
Mo	2.2	32.8	3.15	1.1
Mo/TiO_2(cal)				
O	1.2	36.7	1.97	6.3
S	4.2	60.4	2.39	4.5
Ti	0.3	−4.5	2.97	−1.1
Mo	0.8	16.1	3.16	3.5
Mo/TiO_2(cal) 450°C				
O	1.2	51.1	1.96	−2.6
S	4.6	34.5	2.38	9.1
Ti	0.3	13.8	2.97	8.6
Mo	1.1	1.0	3.15	4.7
$CoMo/TiO_2$(seq)				
O	1.1	73.9	1.96	5.4
S	4.8	16.9	2.40	3.6
Mo	3.4	48.3	3.17	0.6
$CoMo/TiO_2$(co)				
O	0.8	88.4	1.98	0.0
S	5.2	21.1	2.41	2.6
Mo	3.6	40.1	3.15	2.7

has significantly improved at low values of R (1.0 Å $< R <$ 2.0 Å). Both in r- and k-space data and fit agree very well (Fig. 7c), indicating that contributions of higher shells are almost absent as expected in case of small particles.

DISCUSSION

Structure of the Molybdenum Oxide Phase

The analysis results of the EXAFS data of the oxidic catalysts indicate that both on Al_2O_3 and TiO_2 a highly distorted octahedrally coordinated molybdenum oxide species is formed. The height of the preedge peak might additionally point to partial incorporation of Mo in tetrahedral molybdenum oxide species, especially for the Al_2O_3 samples, although this amount will be very small. The structure of molybdenum oxide on several oxidic supports has been extensively described by several authors; see, for example, Wachs *et al.* (46–47) and references therein. It was found that at high surface coverages of MoO_3 on Al_2O_3 a mixture of tetrahedrally and octahedrally coordinated Mo species are present. On TiO_2 only a distorted octahedrally coordinated surface species was found. These findings are consistent with our XAFS results. Raman spectroscopy indicates the presence of the short Mo=O bond, independent of the nature of the support. The EXAFS analyses indicate for most samples the presence of a short Mo−O distance around 1.71 Å. This Mo−O bond might well correspond to a double bonded Mo=O as a similar distance was found for Mo=O bonds in Mo dimers attached to a SiO_2 surface (48). The coordination numbers for this contribution vary between 0.7 ($CoMo/TiO_2$(seq)) and 2.3 ($CoMo/TiO_2$(co)) which is reasonable, compared to the coordination number of 1.9 in MoO_3. Remarkably, Mo/Al_2O_3(cal), Mo/TiO_2(nc), and Mo/TiO_2(cal) have only two Mo−O contributions, instead of three, as found in the other samples. In these catalysts the Mo−O contributions at 1.77 Å and 1.71 Å cannot be separated resulting in one contribution at an intermediate distance between 1.73–1.76 Å.

The dispersion of the molybdenum oxide species on the support is represented by the coordination number of the second shell N_{Mo-Mo}. Comparison of N_{Mo-Mo} for Mo/Al_2O_3(nc) and Mo/Al_2O_3(cal) shows that the

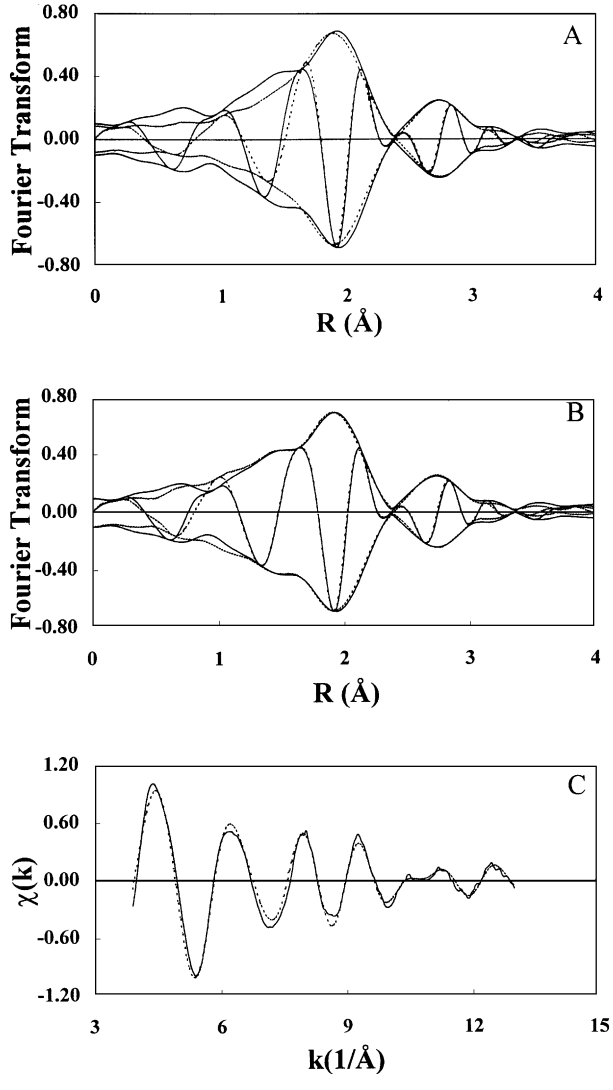

FIG. 7. Sulfided Mo/TiO_2(cal): (a) Fourier transform (———) and three-shell fit (- - -) [k^2, $\Delta k = 3.9-13.0$]; (b) Fourier transform (———) and four-shell fit (- - -) [k^2, $\Delta k = 3.9-13.0$] (cal) EXAFS spectrum (———) and four shell-fit in k-space (- - -).

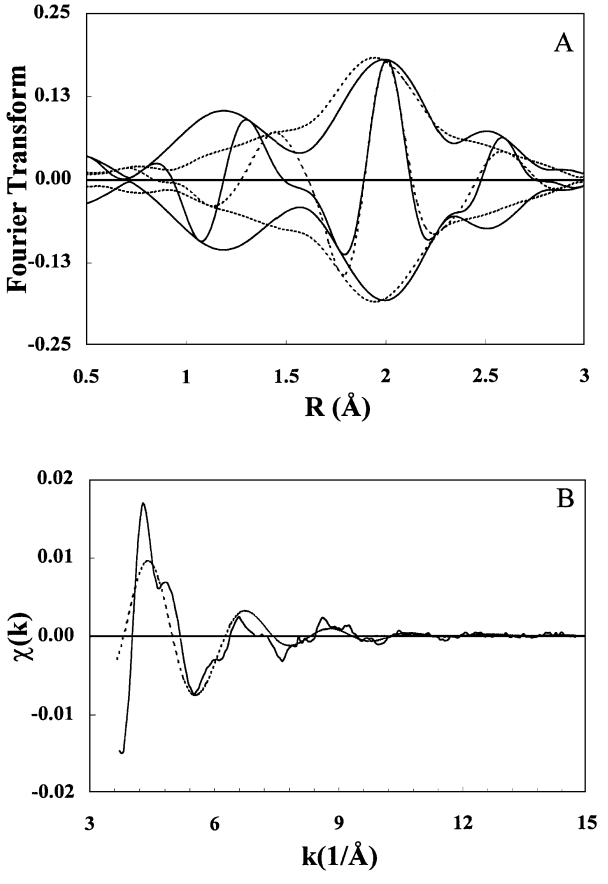

FIG. 8. Mo–O contribution in sulfided Mo/TiO_2(cal): EXAFS spectrum minus calculated Mo–S, Mo–Mo, and Mo–Ti contributions (———) and fit with calculated Mo–O contribution (- - -): (a) Fourier transform [k^2, $\Delta k = 3.9-13.0$ Mo–O phase corrected]; (b) data in k-space (no weighing).

dispersion slightly increases upon calcining. In case of TiO_2 the opposite happens and the molybdenum oxide particles sinter when calcined at 450°C. It seems that the molybdenum oxide particles have a greater affinity for an Al_2O_3 than for TiO_2 surface, probably due to a better "match" of the molybdenum oxide structure on the surface structure of Al_2O_3. The increase in N_{Mo-Mo} for both Mo/Al_2O_3(cal) and Mo/TiO_2 when Co is present indicates that Co promotes sintering of the molybdenum oxide species. No difference is observed whether Co is impregnated sequentially after or together with the Mo precursor. However, the molybdenum oxide particles formed are still very small. For the largest value of N_{Mo-Mo} of 2.54 for $CoMo/TiO_2$(co) it can be calculated that less than four Mo atoms are present per particle (49). The extremely low value of 0.35 for Mo/Al_2O_3(cal) suggests that in this sample almost isolated molybdenum-oxygen clusters are present on the surface of the support.

The interaction between the surface of the support and the molybdenum oxide species can be described to consist of Mo–O-X bonds in which X represents the metal atom of the support (48–50). From the analysis results of the Mo–O contributions it is not directly possible to assign a distinct Mo–O distance to a Mo–O-X bond. Yet, the interaction between the molybdenum oxide particles and the support clearly manifests itself in the presence of a Mo-X contribution in both Mo/Al_2O_3 as Mo/TiO_2 catalysts. The average Mo–O–Al distance of 2.74 ± 0.02 Å found in the alumina catalysts is in agreement with the distance of 2.785 Å for Mo-X found by Kisfaludi *et al.* (51) in the EXAFS analysis of calcined MoO_3/Al_2O_3. The authors proposed this Mo-X distance to correspond with a Mo–Al contribution in a Mo–O–Al configuration. The average distance of 2.87 ± 0.035 Å found in the titania catalysts for Mo–Ti agrees with proposed Mo–Ti contributions in the spectra of MoO_3/TiO_2 by Fay *et al.* (52) and Shimada *et al.* (53). The absence of a Mo–Ti contribution in Mo/TiO_2(nc) can be explained by the poor interaction between the surface of the TiO_2-support and the molybdenum precursor. Although calcining induces sintering of the oxide particles the "intimacy" between support and oxide in enhanced, which leads to the observation of a Mo–Ti contribution in Mo/TiO_2(cal).

One could expect that the dispersion of the molybdenum oxide particles (N_{Mo-Mo}) and the Mo-X contribution are correlated. Close inspection of the coordination numbers for Mo–Mo and Mo-X (X = Ti or Al), however, shows no such relation. As can be seen from Figs. 6 and 7 the fits of the difference files are not optimal due to the structural complexity and variety of the molybdenum oxide species and the interaction with the support. The uncertainty of 20% in the absolute values of coordination number and Debije–Waller factor of Mo-X might well explain the absence of the expected correlation.

Structure of the Molybdenum Sulfide Phase and Sulfide-Support Interaction

The distances found for the Mo–S and Mo–Mo shells are (within limits of accuracy) equal to the distances found for MoS_2 (42). The values for N_{Mo-S} vary between 4 and 5.5 which is substantially lower than the coordination by six sulfur neighbours as in bulk MoS_2. Assuming a S/Mo stoichiometry of 2 and a stacked configuration of the sulfur atoms Bouwens *et al.* (15) calculated the Mo–S coordination to be between 4 and 5 for particle sizes with N_{Mo-Mo} varying between 2 and 4, which is in agreement with our results. Additionally Startsev (14) argued on the basis of the electro-neutrality principle that molybdenum atoms in small MoS_2 particles cannot fully be coordinated by sulfur atoms because of excess negative charge that otherwise would accumulate on the slabs.

Analysis of the second shell of Mo/Al_2O_3(cal) results in a N_{Mo-Mo} of 2.4. The coordination number of the second shell can be used as a direct measure of the two-dimensional size of the particle. With the use of a simple hexagon model

to represent a MoS_2-slab a N_{Mo-Mo} of 2.4 is calculated to correspond with approximately four Mo atoms per slab, which is indeed very small (54). Some authors have questioned the use of N_{Mo-Mo} to estimate the slab size due to the correlation between coordination number and the Debije–Waller factor (13). However, by simultaneous optimization of the fit parameters for both the k^1 and k^3 weighted EXAFS spectra unique values can be found for coordination number N and Debije–Waller factor σ (55). The Debije–Waller factor then expresses the structural disorder of the particles including both thermal disorder and static disorder.

Yet, what can stabilise MoS_2 particles containing only 4–15 Mo atoms per slab as present in our catalysts? The most obvious explanation for stabilisation of these small particles is the linkage of the MoS_2 particles to the support via Mo–O-X bonds. Both for the calcined TiO_2 and Al_2O_3 catalysts a Mo–O contribution at 2.0 Å is observed in the Fourier transform of the sulfided catalysts, which could well be ascribed to such a Mo–O-X linkage. As can be seen in Fig. 9 both for Mo/Al_2O_3 and Mo/TiO_2 the Mo–O contribution increases with increasing MoS_2 dispersion (decreasing Mo–Mo coordination). In our opinion this directly indicates that the observed Mo–O contribution can be assigned to the proposed interfacial MoS_2-support bonds. The distance of 2.0 Å is also in good agreement with the predicted value of 1.85 Å for the Mo–O–Al bond in MoS_2/Al_2O_3 obtained with molecular modelling by Diemann *et al.* (27), taken into account the inhomogenity of the γ-Al_2O_3 and TiO_2 surfaces. Figure 9 shows that in case of the Mo/TiO_2 catalysts a maximum Mo–O contribution of 1 is reached at very small particle sizes. It is very likely that this maximum is related to the geometrical structure of the MoS_2 particles on the support. The orientation of the MoS_2 slabs on the surface of the support then plays an important role. Hayden *et al.* (23) concluded on basis of electron microscopy results that MoS_2 slabs are bonded to the alumina support via their (2110) edge plane. On basis of molecular modelling experiments Diemann *et al.* (27) pictured the MoS_2 slabs bonded on the 110 surface of γ-Al_2O_3 through their (1100) edges with the Mo–O distance of 1.85 Å. Our results indicate a similar result as it is observed that N_{Mo-S} increases with increasing particle size (N_{Mo-Mo}). If the slabs were bonded to the support through their basal plane the average sulfur coordination of the Mo-atoms would not change with increasing slab size. In edge-bonded slabs, however, where only the Mo atoms near the edge are in contact with the support the average sulfur coordination rises with increasing N_{Mo-Mo}. Picturing very small particles of two or three Mo-atoms it is reasonable to assume that at first grow will take place along the surface of the support or "the edge site," which leaves the N_{Mo-O} at a constant value as observed. Only if growth takes place "away" from the surface of the support the N_{Mo-O} will start to decrease as observed for higher coordination numbers N_{Mo-Mo} (see Fig. 9).

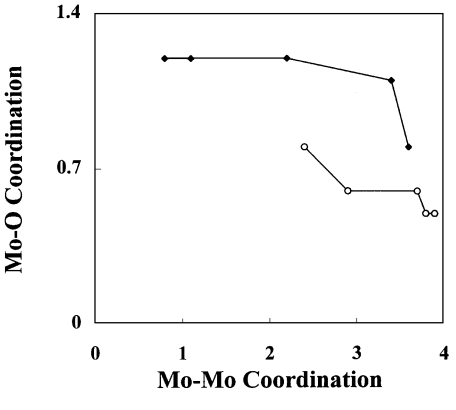

FIG. 9. N_{Mo-O} versus N_{Mo-Mo} for the sulfided Mo/TiO_2 (◆) and Mo/Al_2O_3 (O) catalysts.

Comparison of Mo/Al_2O_3(cal) and Mo/TiO_2(cal) shows that although the molybdenum oxide species are more dispersed on Al_2O_3 the MoS_2 particles formed are smaller on TiO_2. The correlation between N_{Mo-Mo} and N_{Mo-O} is also different for both supports as displayed by Fig. 9. This points to a different geometrical structure of the MoS_2 particles on TiO_2 than on Al_2O_3. Probably the "match" of the MoS_2 edge plane onto the surface of the support is better for titania than alumina. This might result in the growth of the MoS_2 particles on TiO_2 in the direction along the surface while on Al_2O_3 particle growth takes place in all directions. This can explain the observed lower values of N_{Mo-O} on the Al_2O_3 support. A possible structure of a MoS_2 cluster containing seven Mo atoms supported on the [110] plane of γ-alumina (spinel structure, $a_0 = 820$ pm) is visualized in Fig. 10. The MoS_2 cluster is an outtake of the MoS_2 crystal lattice and is positioned in such a way that the Mo atoms are in close contact with the upstanding oxygen row of the alumina plane. Figure 11 presents a similar representation of the same MoS_2 cluster supported on a rutile [110] plane, this plane is a reasonable representation of the titania surface (56). For the Mo atoms able to see the Ti atoms of the support, as indicated by the EXAFS data, it is necessary to locate the MoS_2 cluster on the so called oxygen B-row of the support. The Ti atom is located just beneath the oxygen atoms as depicted in Fig. 11. Remarkably the distance of 2.96 Å between the oxygen atoms in the B-row is close to the 3.16 Å Mo–Mo distance in MoS_2, whereas the oxygen atoms in alumina are separated by 2.60 Å. This might support the proposed better "match" of MoS_2 on titania over alumina, for reasons of lesser strain between the MoS_2 structure and the support in case of titania. However, these visualisations are very qualitative and additional molecular modelling should be done to shed some more light on the exact structure of small MoS_2 particles on both support materials.

As to the origin of the $Mo-O_{support}$ bond it is quite likely that the Mo–O contribution between 1.88 and

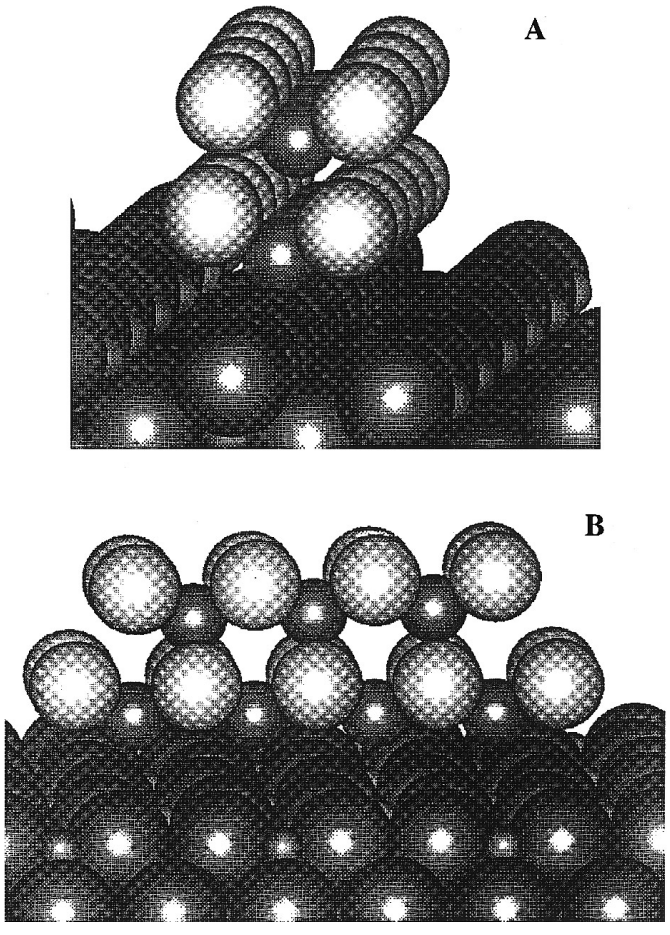

FIG. 10. Representation of a MoS_2 cluster supported on a γ-alumina [110] plane: (a) top view; (b) side view.

1.94 Å as found in the oxidic catalysts represents the same $Mo{-}O_{support}$ contribution. Upon sulfidation the structure of the molybdenum oxide is changed into the sulfide which causes a lengthening of this $Mo{-}O_{support}$ distance. This assumption can only be validated by means of analysis of all subsequent stages in the sulfidation process, which will be described in a following paper.

However, it is very clear that the observed Mo–O contribution at 2.0 Å can be ascribed to an interfacial $Mo{-}O_{support}$ linkage. Moreover, the Fourier transform of the most disperse Mo/TiO_2(cal) catalyst contains an Mo–Ti contribution, which shows the closeness of the Mo atoms in MoS_2 and the Ti atoms of the support. The importance of the Mo–O bonds in stabilising the small MoS_2 particles is shown by comparison of both Mo/Al_2O_3(cal) and Mo/TiO_2(cal) sulfided at 400 and 450°C, respectively. When the Mo–O linkages are sulfided (decreasing N_{Mo-O}) the size of the MoS_2 slabs significantly increases. This means that the dispersion and thereby the activity of these catalysts can be tuned by a controlled sulfidation of the oxidic precursors. EXAFS can be used to monitor the amount of Mo–O support linkages that are left, which maintain the dispersion of the metal sulfide phase.

Effect of Calcining and Presence of Cobalt

Comparison of the sulfided samples of the calcined and noncalcined Mo/Al_2O_3 shows that the MoS_2 dispersion in the calcined sample is slightly better. As the analysis results of the oxidic catalysts indicated that smaller molybdenum oxide particles are formed upon calcining, this can be ascribed to an enhanced Mo-support interaction. Calcination promotes the formation of more Mo–O–Al bonds resulting in smaller oxide particles after calcination, which sulfidic counterparts are more resistant towards sintering because of their stronger linkage to the support. Looking at the sulfided TiO_2 catalysts a similar effect is observed. However, calcination leads to larger molybdenum oxide particles on the calcined sample compared to the Mo/TiO_2(nc) sample. Therefore, the final formation of smaller MoS_2 particles on the sulfided Mo/TiO_2(cal) catalyst must be due to a redispersion of the Mo phase during sulfidation.

The addition of Co to the Mo/Al_2O_3 catalysts does not cause a significant increase in N_{Mo-Mo}. There is no formation of larger sulfide particles as might be expected from the larger molybdenum oxide particles present in the Co promoted catalysts relative to the unpromoted catalyst. With the titania supported Mo catalysts the addition of Co leads to much more pronounced results: the N_{Mo-Mo} increases from 1.1 to an average value of 3.5 for the promoted catalysts. Evidently Co disturbs the interaction between the MoS_2 particles and the support which causes the particles to grow.

As shown in Tables 5 and 6 no Co backscatterer contribution could be found for both the alumina and titania catalysts as found in catalysts containing the so-called "CoMoS" phase (15). Incorporation of a Mo–Co contribution at 2.80 Å did not lead to significant improvement of

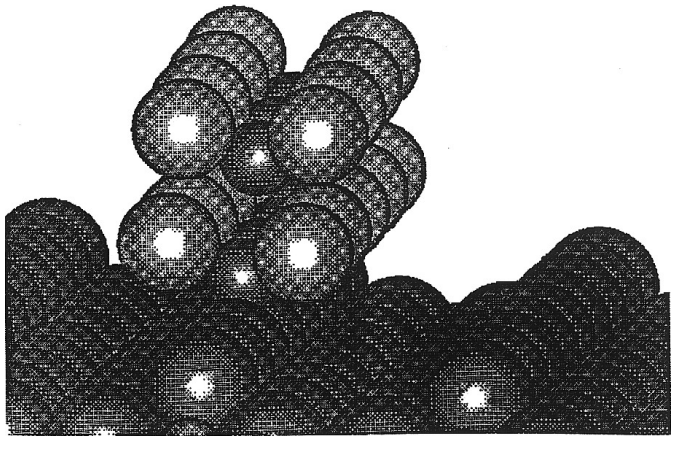

FIG. 11. Representation of a MoS_2 cluster supported on a titania rutile [110] plane.

the fits. As only the Mo atoms at the MoS_2 edges are in contact with Co the Mo–Co contribution is by itself not very pronounced. Moreover, in these samples the interaction between Co and Mo was not optimised to obtain a maximum amount of "CoMoS" phase. For these reasons the absence of a Mo–Co contribution does not contradict the proposed model of Co supported on the MoS_2 edges.

CONCLUSIONS

The main finding of our study is that XAFS enabled us to describe the interface between the active phase and the support in sulfided Mo on alumina and titania catalysts. The interaction between the MoS_2 particles and the surface of the support consists of Mo–O-X (X = Al or Ti) bonds with a Mo–O bond length of 2.0 Å. These Mo–O-X bonds are already present in the fresh oxidic catalysts, as indicated by the presence of second shell Al and Ti neighbours in the Fourier transform. The Mo–O-X bonds are crucial in stabilizing the small MoS_2 particles and prevent them from sintering. The amount of these interfacial Mo–O bonds is higher on titania than on an alumina support. Addition of Co leads to a strong disturbance of the metal–sulfide support interaction on titania and due to this growth of the MoS_2 particles, while on alumina hardly any effect is observed. The dispersion and activity of these catalysts can be controlled by a careful sulfidation procedure, as to maintain the Mo–O bonds between MoS_2 particles and support.

ACKNOWLEDGMENTS

Gert van Dorssen and Barbara Mojet are acknowledged for their help with performing the EXAFS experiments in Daresbury and Jaap Louwen for creating the computer models. Akzo-Nobel Research Center Amsterdam is gratefully acknowledged for their financial support for the in situ EXAFS cells and gasflow equipment.

REFERENCES

1. Massoth, F. E., *Adv. Catal.* **27**, 265 (1978).
2. Gates, B. C., Katzer, J. R., and Schuit, G. C. A., "Chemistry of Catalytic Processes." McGraw–Hill, New York, 1979.
3. Ratnasamy, P., and Sivasanker, S., *Catal. Rev. Sci. Eng.* **22**(3), 401 (1980).
4. Grange, P., *Catal. Rev. Sci. Eng.* **21**(1), 135 (1980).
5. Keely, W. M., Jerus, P., Dienes, E. K., and Hausberger, A. L., *Catal. Rev. Sci. Eng.* **26**(3, 4), 485 (1984).
6. Dellanay, F., *Appl. Cat.* **16**, 135 (1985).
7. Topsøe, H., Clausen, B. S., Topsøe, N. Y., and Pedersen, E., *Ind. Eng. Chem. Fund.* **25**, 25 (1986).
8. Topsøe, H., and Clausen, B. S., *Appl. Cat.* **25**, 273 (1986).
9. Prins, R., de Beer, V. H. J., and Somorjai, G. A., *Catal. Rev. Sci. Eng.* **31**(1, 2), 1 (1989).
10. Luck, F., *Bull. Soc. Chim. Belg.* **100**(11, 12), 781 (1991).
11. Breysse, M., Portefaix, J. L., and Vrinat, M., *Catal. Today* **10**, 489 (1991).
12. Delmon, B., *Catal. Lett.* **22**, 1 (1993).
13. Chianelli, R. R., Daage, M., and Ledoux, M. J., *Adv. Catal.* **40**, 177 (1994).
14. Startsev, A. N., *Catal. Rev. Sci. Eng.* **37**(3), 353 (1995).
15. Bouwens, S. M. A. M., Prins, R., de Beer, V. H. J., and Koningsberger, D. C., *J. Phys. Chem.* **94**, 3711 (1990).
16. Bouwens, S. M. A. M., van Veen, J. A. R., Koningsberger, D. C., de Beer, V. H. J., and Prins, R., *J. Phys. Chem.* **95**, 123 (1991).
17. Bouwens, S. M. A. M., van Zon, F. B. M., van Dijk, M. P., van der Kraan, A. M., de Beer, V. H. J., van Veen, J. A. R., and Koningsberger, D. C., *J. Phys. Chem.* **146**, 375 (1994).
18. Crajé, M. W. J., de Beer, V. H. J., and van der Kraan, A. M., *Bull. Soc. Chim. Belg.* **100**, 953 (1991).
19. Crajé M. W. J., de Beer, V. H. J., and van der Kraan, A. M., *Appl. Cat.* **70**, L7 (1991).
20. Candia, R., Sørensen, O., Villadsen, J., Topsøe, N. Y., Clausen, B. S., and Topsøe, H., *Bull. Soc. Chim. Belg.* **93**(8, 9), 763 (1984).
21. Stockmann, R. M., Zandbergen, H. W., van Langeveld, A. D., and Moulijn, J. A., *J. Mol. Catal. A* **102**, 147 (1995).
22. Louwers, S. P. A., Crajé M. W. J., van der Kraan, A. M., Geanet, C., and Prins, R., *J. Catal.* **144**, 579 (1993).
23. Hayden, T. F., and Dumesic, J. A., *J. Catal.* **104**, 366 (1987).
24. Chiu, N.-S., Bauer, S. H., and Johnson, M. F. L., *J. Catal.* **98**, 32 (1986).
25. Shimada, H., Matsubayashi, N., Sato, T., Yoshimura, Y., Imamura, M., Kameoka, T., and Nishijima, A., *Catal. Lett.* **20**, 81 (1993).
26. Derouane, E. G., Pedersen, E., Calusen, B. S., Gabelica, Z., Candia, R., and Topsøe, H., *J. Catal.* **99**, 253 (1986).
27. Diemann, E., Weber, Th., and Müller, A., *J. Catal.* **148**, 288 (1994).
28. Muñoz-Páez, A., and Koningsberger, D. C., *J. Phys. Chem.* **99**, 4193 (1995).
29. Ng, K. Y. S., and Gulari, E., *J. Catal.* **95**, 33 (1985).
30. Shimada, H., Sato, T., Yoshimura, Y., Hiraishi, J., and Nishijima, A., *J. Catal.* **110**, 275 (1988).
31. Moulijn, J. A., van Doorn, J., van Langeveld, A. D., Mangus, P. J., Tajik, S., de Beer, V. H. J., Barthe-Zahir, N., Bouwens, S. M. A. M., van Gestel, J. N. M., van Oers, E. M., van der Kraan, A. M., Crajé M. W. J., and Ramselaar, W. L. T. M., *Int. J. Energy. Res.* **18**, 127 (1994).
32. Kampers, F. W. H., Maas, T. M. J., Van Grondelle, J., Brinkgreve, P., and Koningsberger, D. C., *Rev. Sci. Instrum.* **60**, 2635 (1989).
33. Van Zon, J. B. A. D., Koningsberger, D. C., Van Blik, H. F. J., and Sayers, D. E., *J. Chem. Phys.* **82**, 5742 (1985).
34. Duivenoorden, F. B. M., Koningsberger, D. C., Uh, Y. S., and Gates, B. C., *J. Am. Chem. Soc.* **108**, 6524 (1986).
35. Kampers, F. W. H., Engelen, C. W. R., Van Hooff, J. H. C., and Koningsberger, D. C., *J. Phys. Chem.* **94**, 8574 (1990).
36. Lytle, F. W., Sayers, D. E., and Stern, E. A., *Physica B* **158**, 701 (1988).
37. Stern, E., Newville, M., Ravel, B., Yacoby, Y., and Haskel, D., *Physica B* **208/209**, 117 (1995).
38. Kutzler, F. W., Natoli, C. R., Misemer, D. K., Doniach, S., and Hodgson, K. O., *J. Phys. Chem.* **73**, 3274 (1980).
39. Mensch, C. T. J., van Veen, J. A. R., van Wingerden, B., and van Dijk, M. P., *J. Phys. Chem.* **92**, 4961 (1988).
40. Shulman, R. G., Yafet, Y., Eisenberger, P., and Blumber, W. E., *Proc. Natl. Acad. Sci. USA* **73**(5), 1384 (1976).
41. Matsumoto, K., Kobayashi, A., and Sasaki, Y., *Bull. Chem. Soc. Jpn* **48**, 1009 (1975).
42. Kihlborg, L., *Ark. Kemi* **21**, 357 (1963); cf. *Structure Rep.* **28**, p. 128.
43. Hayes, T. M., and Boyce, J. B., *Solid State Phys.* **37**, 173 (1982).
44. Bauchspiess, K. R., *Jpn. J. Appl. Phys.* **32**(2), 131 (1993).
45. Dickinson, R. G., and Pauling, L., *J. Am. Chem. Soc.* **45**, 1466 (1923).
46. Hu, H., Wachs, I. E., and Bare, S. R., *J. Phys. Chem.* **99**, 10897 (1995).

47. Kim, D. S., Wachs, I. E., and Segawa, K., *J. Catal.* **146**, 268 (1994).
48. Iwasawa, Y., *Catal. Today* **6**, 27 (1989).
49. de Boer, M., Ph.D. thesis, p. 65, Utrecht, 1992.
50. Rajagopal, S., Marzari, J. A., and Miranda, R., *J. Catal.* **151**, 192 (1995).
51. Kisfaludi, G., Leyrer, J., Knözinger, H., and Prins, R., *J. Catal.* **130**, 192 (1991).
52. Fay, M. J., Proctor, A., Hoffmann, D. P., Houalla, M., and Hercules, D. M., *Mikrochim. Acta* **109**, 281 (1992).
53. Shimada, H., Matsubayashi, N., Sato, T., Yoshimura, Y., and Nishijima, A., *J. Catal.* **138**, 746 (1992).
54. de Boer, M., van Dillen, A. J., Koningsberger, D. C., and Geus, J. W., *J. Phys. Chem.* **98**, 7862 (1994).
55. Kampers, F. W. H., Ph.D. thesis, Eindhoven, 1989.
56. Huisman, H. M., Ph.D. thesis, Utrecht, 1994.